

Simulations of the kinetic friction due to adsorbed surface layers

Gang He and Mark O. Robbins

Department of Physics & Astronomy, Johns Hopkins University
E-mail: mr@pha.jhu.edu

Received 11 August 2000

Simulations of the kinetic friction due to a layer of adsorbed molecules between two crystalline surfaces are presented. The adsorbed layer naturally produces friction that is consistent with Amontons' laws and insensitive to parameters that are not controlled in experiments. The kinetic friction rises logarithmically with velocity as in many experimental systems. Variations with potential parameters and temperature follow variations in the static friction. This correlation is understood through analogy with the Tomlinson model and the trends are explained with a hard-sphere picture.

Keywords: kinetic friction, Amontons' laws, surface layers, molecular dynamics, simulations

1. Introduction

One of the major challenges for researchers in the field of nanotribology is to uncover the molecular origins of macroscopic behavior. For example, why do many systems obey Amontons' laws that friction is proportional to normal load L and independent of the apparent geometric area of the surfaces A_{app} ? Unfortunately many simple molecular scale models give results that are qualitatively inconsistent with macroscopic measurements [1,2,3,4,5,6,7,8,9,10,11]. Indeed they suggest that static friction should almost never be observed [5,6,7,8,9,10,11]! A possible origin for such discrepancies [6,12,13,14] is that the models consider contacts between two bare surfaces. Real surfaces almost always have an intervening layer of material called "third bodies" [15,16,17]. This layer may be dust, grit, wear debris, or the few angstroms of hydrocarbons and water that adsorb rapidly on surfaces that are exposed to air.

In a recent paper He *et al.* [12] explored the effect of adsorbed layers on the static friction F_s . They showed that such layers naturally lead to a non-vanishing F_s that exhibits much of the behavior seen in macroscopic experiments. For example the calculated value of F_s is insensitive to many parameters that are not controlled in experiments, including crystallographic alignment, the thickness of the adsorbed layer, and the precise size of the molecules. More importantly, the simulation results provided a molecular basis for Bowden and Tabor's phenomenological explanation of Amontons' laws [18].

Bowden and Tabor had noted that A_{app} is usually much larger than the area of intimate molecular contact A_{real} . They pointed out that both Amontons' laws and many exceptions to them could be explained *if* the local shear stress τ in the contacts increased linearly with the

local pressure P :

$$\tau = \tau_0 + \alpha P \quad . \quad (1.1)$$

Summing over A_{real} and dividing by load gives a friction coefficient

$$\mu \equiv F/L = \alpha + \tau_0/P. \quad (1.2)$$

This is independent of load if P is constant or $\tau_0/P \ll \alpha$. Later work showed that both elastic[19,20] and plastic[18] models of surfaces with many contacts yield a constant P at high loads. At low loads, P decreases, explaining why many systems show an increase in μ in this limit [18,21].

He *et al.*'s work [12] showed that adsorbed layers lead to a static friction that obeys Eq. 1.1. However, most experiments measure the kinetic friction. Although experimental values for the two quantities are often correlated, it is not obvious that they should be. Static friction is the threshold force that must be overcome before one solid slides over another. It arises because the two bodies have locked together into a local energy minimum, and F_s is the force needed to break them free from this minimum. Kinetic friction $F_k(v)$ is the force needed to maintain sliding at a given velocity v . As such it is proportional to the work that must be done due to energy dissipation during sliding. Thus kinetic and static friction involve different phenomena and they have very different values in many simple models [1,2,3,4,5,6,7,8,9,10,11].

In this paper we consider the effect of adsorbed layers on kinetic friction. We first show that the linear relation in Eq. 1.1 is obeyed for each velocity. The intercept τ_0 is relatively independent of velocity below about 1 m/s. The slope α shows a logarithmic dependence on velocity over more than two decades in velocity. This same functional dependence is observed in

experiments, and used in rate-state models of friction [22,23,24]. We next examine the effect of interaction potentials, temperature, and crystallographic alignment on kinetic friction. The variations with these parameters are consistent with a simple hard sphere model for lateral forces. We conclude by considering the strong correlation between calculated values of F_k and F_s . A qualitative explanation for this correlation is suggested based on results for the Tomlinson model [1], and this analogy is confirmed by detailed analysis of the dynamics of individual molecules.

The following section describes the model we use for the surfaces and the intervening molecular layer. The next section presents results, and the final section provides a summary and conclusions.

2. Computational Methodology

Since our goal is to establish general mechanisms, we use relatively simple interaction potentials in our simulations. These allow us to quickly span a wide range of sliding velocities, system sizes, geometries and interactions. They also allow treatment of longer time and length scales than more detailed potentials.

We find similar behavior for both crystalline and disordered walls [12,13,14]. For the results described below, each solid contains discrete atoms forming the (111) surface of an fcc crystal. The coordinate system is chosen so that the surfaces lie in the $x-y$ plane, and periodic boundary conditions are applied in these directions to minimize edge effects. Note that the periodic boundary conditions also prevent us from considering perfectly incommensurate systems. However, we find that surfaces exhibit incommensurate behavior as soon as the common period becomes longer than a few lattice constants [13].

The two opposing surfaces have approximately the same nearest-neighbor spacing d_{nn} , and the effect of commensurability is explored by rotating the top surface by an angle θ about the z -axis. A discrete set of angles is studied that allow both surfaces to retain their hexagonal symmetry. Except where noted, the bottom wall has $d_{nn} = 1.2\sigma$. The value of d_{nn} for the top wall is adjusted slightly ($\leq 2.1\%$) in order to satisfy the periodic boundary conditions. No correlation between the size of this adjustment and the calculated friction was seen at the level of the statistical fluctuations.

Atoms in the bottom solid are fixed in place, and atoms in the top solid translate together as a rigid body of mass M . Previous work shows that including elastic deformations of the solids produces a slightly lower static friction [12,13,25], and we find a similar reduction in the kinetic friction. A constant downward pressure is applied to the top solid, and its height varies in response to this external pressure and molecular interactions. A constant lateral force or velocity is applied along the

nominal sliding direction, usually \hat{x} . The wall is free to move in the other lateral direction, i.e. the external force is zero in this direction. The kinetic friction is determined by imposing a constant lateral velocity v , and calculating the average opposing force. This average is performed over a displacement of at least $25d_{nn}$ in order to reduce statistical fluctuations. The static friction is obtained by applying a constant lateral force, and determining the value needed to initiate sliding [12].

The layer of molecules between the solids is described with a bead-spring model. Previous studies have shown that this model yields realistic dynamics for polymer melts [26], and shown how to map between it and detailed chemical models of polymers [27,28]. These detailed models take at least an order of magnitude more computer time.

Each molecule contains n spherical monomers of mass m . We considered simple spherical molecules $n = 1$, and short chains that model airborne hydrocarbons, $n = 3$ and 6 . All monomers interact through a truncated Lennard-Jones potential [29]:

$$V_{LJ}(r) = 4\epsilon [(\sigma/r)^{12} - (\sigma/r)^6] \quad \text{for } r < r^c, \quad (2.1)$$

where r is the distance between molecules and the potential is zero for $r > r^c$. Adjacent monomers along a chain are coupled by an additional potential that prevents chains from crossing or breaking:

$$V_{CH}(r) = -(1/2)kR_o^2 \ln[1 - (r/R_o)^2] \quad , \quad (2.2)$$

where $R_o = 1.5\sigma$ and $k = 30\epsilon/\sigma^2$ [26]. The parameters ϵ , σ , and $t_{LJ} \equiv (\sigma^2/m\epsilon)^{1/2}$ are characteristic energy, length, and time scales, respectively. These characteristic scales are used to normalize other quantities. Values that would be representative of hydrocarbons are $\epsilon \sim 30\text{meV}$, $\sigma \sim 0.5\text{nm}$ and $t_{LJ} \sim 3\text{ps}$ [26]. The unit of pressure, $\epsilon\sigma^{-3}$, corresponds to about 40MPa.

Wall atoms interact with monomers through a Lennard-Jones potential with a different cutoff, r_{wf}^c , and different energy and length scales, ϵ_{wf} and σ_{wf} , respectively. This allows us to increase or decrease the amount of adhesion, and the effective surface corrugation of the walls. In most cases we considered purely repulsive interactions: $r^c = 2^{1/6}\sigma$ and $r_{wf}^c = 2^{1/6}\sigma_{wf}$. In this limit, atoms on opposing walls are far enough apart that they do not interact. As shown below, the main effect of increasing the interaction range is to add an extra adhesive pressure between the walls.

All of our runs are done in a constant temperature ensemble. We have performed extensive tests on the effects of thermostats [10,30,31,32]. In the appropriate limits, thermostats prevent a gradual rise in temperature due to frictional dissipation without having a direct influence on the friction force. To ensure that one is in these limits, the thermostat must be applied normal to the sliding direction and be sufficiently weak, and the velocity must be low ($\leq 0.1\sigma/t_{LJ}$). At high velocities,

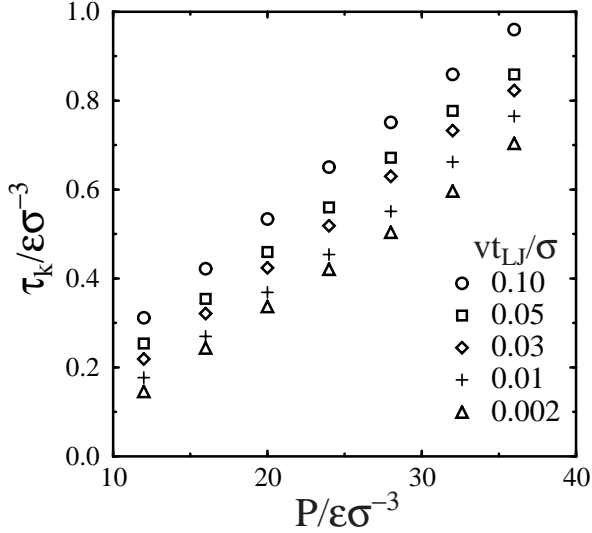


Figure 1. Kinetic shear stress τ_k as a function of pressure for the indicated velocities. Velocities are in units of $\sigma/t_{LJ} \sim 100\text{m/s}$, and the unit of stress and pressure is $\epsilon\sigma^{-3} \sim 40\text{MPa}$. For these runs $\theta = 30^\circ$, $\sigma_{wf} = \sigma$, $\epsilon_{wf} = \epsilon$, $n = 6$, $d_{nn} = 1.2\sigma$, and the number of monomers is equal to the number of atoms on the surface of the bottom wall. The data for each velocity lies on a straight line. We confirmed that linearity extended up to $P/\epsilon\sigma^{-3} = 100$ for the highest velocities.

the structure and other properties of the film may be affected [33,34]. In the following simulations, a Langevin thermostat with damping rate $0.4t_{LJ}^{-1}$ is coupled to the equations of motion in both directions normal to the sliding direction [30,35].

The equations of motion are integrated using a fifth-order Gear predictor-corrector algorithm with a time step $dt = 0.005\sigma/t_{LJ}$. Unless otherwise noted, the area of a periodic unit cell is $\mathcal{A} = 720\sigma^2$ and the mass of the wall is $M/m = 0.8\mathcal{A}/\sigma^2$. Previous studies show that finite-size effects are very small at this system size [25]. Most simulations are done at temperature $T = 0.7k_B/\epsilon$, where k_B is Boltzmann's constant.

3. Results

3.1. Variation with pressure and velocity

Figure 1 shows the pressure dependence of the kinetic friction at the indicated velocities for an incommensurate system, $\theta = 30^\circ$. At each velocity the shear stress τ_k rises linearly with pressure over the entire range of pressures. Using realistic values of ϵ and σ , the highest pressures correspond to about 1.5GPa. The linear relation continues up to $P = 100\epsilon\sigma^{-3}$ in the cases we have tested. However, the larger forces at these pressures require a reduction in the integration time step, making the calculations much slower.

Values of α and τ_0 were obtained from linear fits to data like that shown in Fig. 1. In each case the correlation coefficient was greater than .999. The results

are plotted against the logarithm of velocity in Figure 2. The value of α increases as the logarithm of velocity over the entire range of Fig. 2 – a factor of 200 in v . In contrast, the value of τ_0 becomes independent of velocity for $v < 0.01\sigma/t_{LJ} \sim 1\text{m/s}$. It is negative because these simulations used a purely repulsive potential $r^c/\sigma = 2^{1/6}$. We show later that including adhesive interactions leads to positive values of τ_0 .

A logarithmic variation of friction with velocity is also seen in many experimental systems [22,23,24]. Measured friction coefficients fit a “rate-state” equation:

$$\mu = \alpha + \tau_0/P = \mu_0 + A \ln(v/v^0) + B \ln(\Theta/\Theta^0), \quad (3.1)$$

where Θ is a variable that describes the state of the system, and μ_0 is the friction at the reference velocity v^0 and state Θ^0 . In most cases Θ is treated as a phenomenological parameter whose evolution is described by:

$$d\Theta/dt = 1 - \Theta v/D_c \quad (3.2)$$

where D_c has units of length. Dieterich and Kilgore have shown that changes in Θ are proportional changes in the true area of contact between rough surfaces and that D_c corresponds to the typical diameter of contacts [36].

Our simulations give the dependence of friction on v at fixed contact area [37] and thus the slope of Fig. 2(a) gives $A = 0.00110 \pm 0.00005$. This is smaller than typical experimental values for glass or rocks where A is .005 to .015. However, one might expect A to increase with α . While our values of α are comparable to values for flat crystalline surfaces like mica[38,39] or MoS₂[17], they are much smaller than values for rocks. The ratio A/α is about .05 for our system, and varies from .008 to .025 for rocks. We do not know of any measurements of A for mica or MoS₂, but it would be interesting to see how results for these systems compare to our simulations.

3.2. Variation of μ with interaction potential, T and geometry

A variety of interaction potentials and geometries have been considered to determine which factors influence α and τ_0 and which leave them unchanged. As shown in Fig. 3, doubling the interaction between wall atoms and fluid monomers has almost no effect on the friction. In contrast, the friction increases rapidly with the ratio of d_{nn} to σ_{wf} . For $d_{nn} = 1.2\sigma$ we find α rises from 0.012 to 0.034 as σ_{wf} drops from 1.2 to 0.9. The value of τ_0 increases in magnitude from -0.07 to -0.16. Although not shown, increasing d_{nn} at fixed σ_{wf} also increases α .

These trends in α can be understood from a simple geometrical picture. At the pressures of interest, the interactions are dominated by the repulsive r^{-12} term

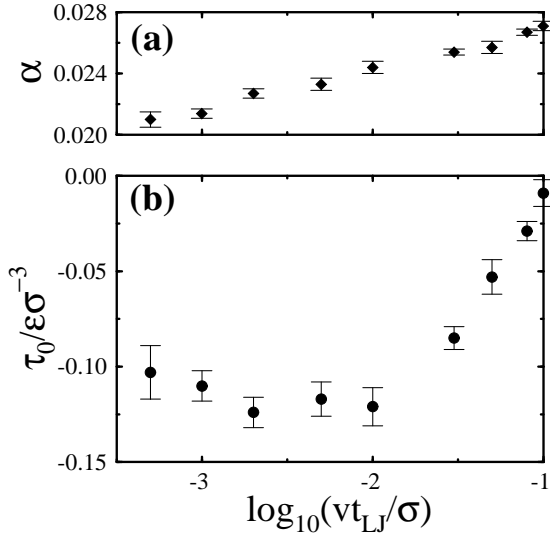


Figure 2. Plot of (a) α and (b) τ_0 against the logarithm of the velocity for the system of Fig. 1.

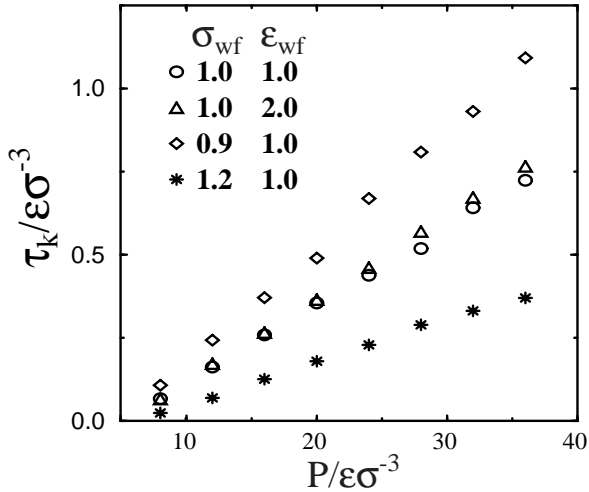


Figure 3. Plot of shear stress against pressure at $v = 0.005\sigma/t_{LJ}$ for the indicated values of σ_{wf} and ϵ_{wf} . Other parameters are the same as for Fig. 1.

in the Lennard-Jones potential. Monomers and wall atoms can be thought of as hard spheres with an effective diameter D that is determined by the separation r at which the Lennard-Jones force balances the force from the applied pressure. This picture gives a diameter $D \propto \sigma_{wf}(\epsilon_{wf}/\sigma_{wf}P)^{-1/13}$, that varies rapidly with σ_{wf} but very little with ϵ_{wf} or P . As illustrated in Fig. 4, monomers can penetrate deep between surface atoms when D/d_{nn} is small. This increases the friction because monomers must be lifted up the ramp formed by the surface of closest approach in order to translate. The required lateral force is the normal load times the slope of the surface which increases as D/d_{nn} decreases. Thus the hard-sphere model explains the linear dependence of τ on pressure as well as the insensitivity to ϵ_{wf}

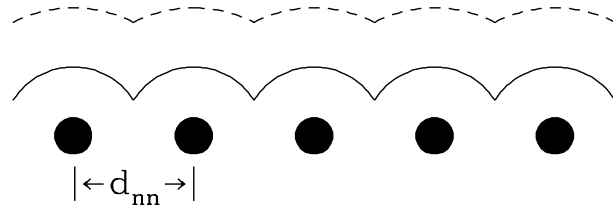


Figure 4. Sketch of surface of closest approach for $D/d_{nn} = 0.7$ (solid line) and 1.3 (dashed line). The lateral force required to lift monomers up the ramps that these surfaces represent is given by the slope times the normal force.

and the variation with σ_{wf} .

The simulations just described were for strictly repulsive potentials ($r_{wf}^c = 2^{1/6}\sigma_{wf}$), and one may wonder whether the hard-sphere picture is more generally applicable. We have done simulations with $r_{wf}^c = 2.2\sigma_{wf}$ to test this. When direct wall/wall interactions are neglected, we find that the kinetic friction is fit by $\alpha = 0.0211 \pm 0.0003$ and $\tau_0 = +0.007 \pm .008$ over a pressure range from 0 to $36\epsilon\sigma^{-3}$ for the parameters of Fig. 1. This value of α is only 8% smaller than for a purely repulsive potential. In contrast, τ_0 increases substantially because the attraction between monomers and wall atoms increases the effective pressure holding them together. Adding direct wall/wall interactions leads to a slightly larger adhesive pressure, and a slightly larger value of τ_0 .

The effect of temperature on α is also fairly weak. So far we have shown results for $T = 0.7\epsilon/k_B$, which is near the triple point for spherical Lennard-Jones molecules, and roughly 30% above the glass transition temperature for chain molecules. This temperature was chosen because many airborne hydrocarbons are above their melting point at room temperature. Figure 5 shows the variation of α and τ_0 with temperature at $v = 0.005\sigma/t_{LJ}$ for the system of Figs. 1 and 2. The value of α changes only weakly with temperature, falling about 20% from $k_B T/\epsilon = 0.3$ to 1.2. The high end of this temperature range is more than twice the glass transition temperature for chain molecules and close to the critical temperature for spherical molecules.

The weak variation of α with T is consistent with our geometrical picture, since the hard-sphere diameter is insensitive to temperature. In contrast, the value of τ_0 is roughly proportional to temperature over the studied range. Equation 1.1 implies that the friction vanishes for $P < -\tau_0/\alpha$. Of course this can not happen, but there is a qualitative change in the type of friction as the pressure drops below $-\tau_0/\alpha$. At high pressures we observe static friction and a slightly smaller kinetic friction that rises logarithmically with velocity. For $P < -\tau_0/\alpha$ the static friction vanishes, and the kinetic friction rises from zero as a power of the velocity.

This change in frictional behavior reflects a change in the state of the film that has been studied previously

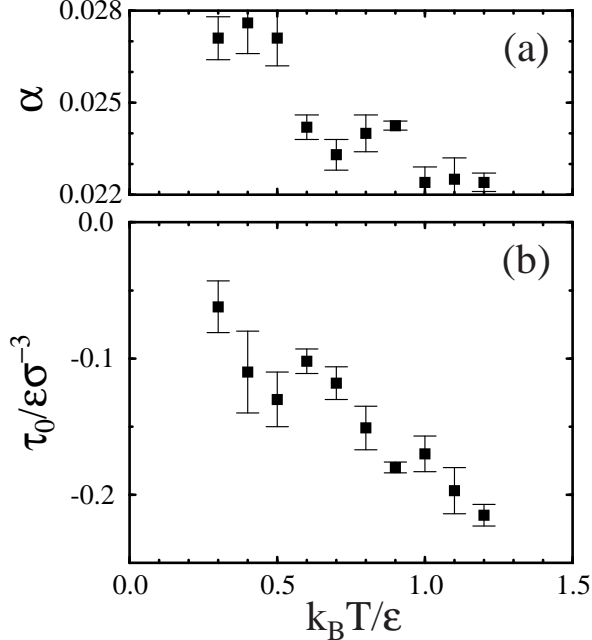


Figure 5. Variation of (a) α and (b) τ_0 with temperature at $v = 0.005\sigma/t_{LJ}$ for the system of Fig. 1.

in multi-layer systems [40,41,42,43,44,45]. At high pressures the molecules lock into a glassy state, while at low pressures they diffuse freely and act like a viscous lubricant. Fig. 5 implies that the pressure required to lock molecules into a glassy state rises linearly with T . This result is specific to our choice of purely repulsive potentials ($r^c = 2^{1/6}\sigma$). Adding an attractive tail to the potential shifts the entire temperature dependent curve upwards, and gives glassy behavior at lower (even negative) pressures. Note that earlier results on multi-layer films indicated that τ was independent of velocity in the glassy state [42]. However, these results covered a relatively small range of v and are not inconsistent with the logarithmic variation seen in Fig. 2.

3.3. Relation to static friction

The changes in kinetic friction with temperature, interaction potential, geometry and other factors are very similar to what we have observed for static friction [12,25]. Indeed the ratio between the value of $\alpha_k(v)$ at a given velocity and the value of α_s for static friction is relatively constant. For example, over the range of temperatures and potential parameters shown in Figures 3 and 5, $\alpha_k(v = 0.005\sigma/t_{LJ})$ is between 75 and 85% of α_s . This variation is comparable to our statistical uncertainties.

Figure 6 illustrates the correlation between static and kinetic friction as θ is varied. Only the range $\theta = 0$ to 30° is shown, since the values at other θ are related by symmetry. The simulation data in previous figures was for $\theta = 30^\circ$ and the commensurate case corresponds to $\theta = 0^\circ$. We confirmed that the friction is linear in P

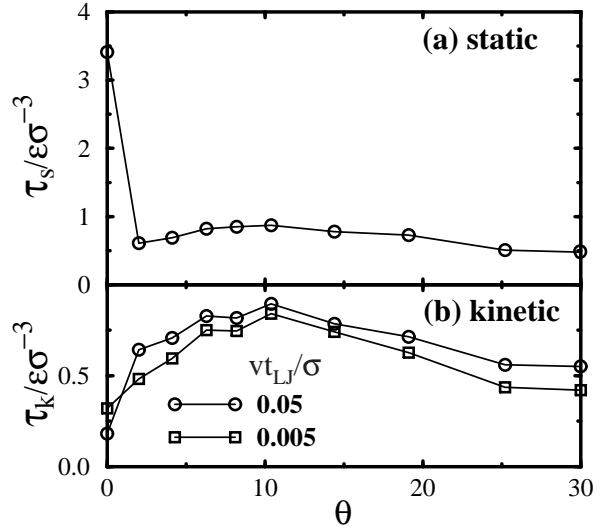


Figure 6. Variation of (a) static and (b) kinetic friction with θ at $P = 24\epsilon\sigma^{-3}$. Error bars in both panels are about 5%. For these simulations the area of the unit cell is $2880\sigma^2$, and the number of monomers is equal to the number of atoms on the surface of the bottom wall.

for several θ , and show results for a single, relatively high pressure ($P = 24\epsilon\sigma^{-3}$) to minimize the number of calculations, and emphasize the contribution from α . Data for a monolayer film is shown because it gives the largest variation in friction with θ and thus the best test of correlations between F_k and F_s [46]. As θ changes from 2° to 30° , F_k varies by almost a factor of two, yet the ratio F_k/F_s stays constant within our statistical uncertainties. For $v = 0.005\sigma/t_{LJ}$ we find $F_k/F_s = 0.88 \pm 0.10$, while $F_k/F_s = 1.05 \pm 0.10$ for $v = 0.05\sigma/t_{LJ}$.

The correlation between F_k and F_s is lost when the walls become commensurate. As θ decreases from 2° to 0° there is a sharp increase in F_s by about a factor of seven, and a drop in F_k by about a factor of two. In addition, there is a qualitative change in the velocity dependence of the kinetic friction: F_k decreases with velocity in the commensurate case, but increases with v for incommensurate walls.

The observed correlation between static and kinetic friction is somewhat surprising given that they reflect different physical effects. As noted in the introduction, the static friction is related to the force needed to pull the system out of a local potential energy minimum, while the kinetic friction is related to the energy dissipated during sliding. Nevertheless, the above comparisons of F_k and F_s indicate that the two arise from similar processes when the walls are incommensurate.

3.4. Comparison to the Tomlinson model

Some insight into the relation between static and kinetic friction is provided by a simple one-dimensional ball and spring model called the Tomlinson model [1,3,10,11]. This model considers two bare surfaces in

contact. The bottom surface is modeled by a sinusoidal potential with amplitude V_0 and period d_{nn} . Atoms in the top surface are treated as independent, overdamped oscillators that are coupled to the center of mass X_{CM} by a spring of stiffness k .

The behavior of the Tomlinson model depends on the dimensionless parameter $\lambda \equiv 4\pi^2 V_0 / k d_{nn}^2$ that measures the relative stiffness of the potential and spring. When λ is small, the spring is so stiff that each atom has only one metastable state at any X_{CM} . In this limit atoms move smoothly over the periodic potential from the bottom wall. This nearly reversible motion leads to little dissipation, and F_k goes to zero linearly with the center of mass velocity [3,10,11]. When λ is large, each atom can get locked in many metastable states at any center of mass position. Each atom starts in one such state. As X_{CM} increases, that state eventually becomes unstable and the atom pops rapidly to the next state. During these pops the system is far from equilibrium and a substantial amount of energy is dissipated. The sequence of pops and the amount of energy dissipated during a given wall displacement ΔX_{CM} is independent of wall velocity in the limit $V_{CM} \rightarrow 0$. Since the dissipated energy equals $F_k(v)\Delta X_{CM}$, the kinetic friction approaches a constant value, $F_k(0)$, in this limit. One can show that $F_k(0)$ approaches the maximum force exerted by the periodic potential $F_{max} \equiv 2\pi V_0 / d_{nn}$ times the number of atoms N as $\lambda \rightarrow \infty$ [3,10,11].

The static friction in the Tomlinson model depends on whether the walls are commensurate or incommensurate [10,11]. In the commensurate case all atoms feel the same periodic potential at each X_{CM} . The maximum force that must be overcome as they advance by a period is $F_s = N F_{max}$. The ratio F_k / F_s vanishes for $\lambda < 1$ and approaches unity as $\lambda \rightarrow \infty$. In the incommensurate case $F_s = 0$ for $\lambda < 1$. For $\lambda > 1$, the static friction is equal to the low velocity kinetic friction. This link between F_s and F_k can be seen by calculating $F_k(0)$ from instantaneous forces rather than the dissipated energy. At very low velocities almost all of the atoms are stuck in a metastable minimum at any instant in time. The force resisting motion, $F_k(0)$, comes from the force exerted by the periodic potential on these atoms. One can show that summing this force or calculating the energy dissipated during atomic pops gives the same answer for F_k [10,11]. For incommensurate walls the distribution of metastable states and thus the lateral force is independent of position. Hence the static friction equals the force $F_k(0)$ needed to advance the wall at a very low velocity.

In most cases two bare surfaces will be incommensurate and the interactions between them will be weaker than their internal interactions. This corresponds to the case $\lambda < 1$ and one expects the static friction and low velocity kinetic friction to vanish [3,4,5,6,7,8,9,10,11]. In contrast, the layer of adsorbed molecules included

in our calculations acts like a very compliant solid with $\lambda > 1$. As expected from the Tomlinson model, this produces a finite static friction and a comparable kinetic friction. The lateral force is predominantly determined by the hard sphere interactions which can be expressed as the normal load times the local slope of the surface of closest approach (Figure 4). Since the surface is nearly independent of load and other parameters, the lateral force is proportional to load and Amontons' laws are obeyed.

We have confirmed the connection between our results and the Tomlinson model by analyzing the motion of individual monomers at low velocities. The number of particles that move by more than a distance c over a time interval of $2t_{LJ}$ is calculated as a function of c . This time interval is chosen because it is longer than the velocity-velocity autocorrelation time and the typical period of oscillations of individual monomers about their metastable minima. We focus on the case where the film is in a glassy state and static friction is observed ($P > -\tau_0/\alpha$).

In equilibrium ($v = 0$), the distribution of monomer displacements is consistent with thermal motion about metastable minima plus extremely slow diffusion of monomers between metastable minima. When the top wall is advanced at a low velocity, almost all of the monomers are locked in local metastable minima during any short time interval. As in the Tomlinson model, they provide almost all of the force on the top wall and thus determine F_k . Monomers that advance by significantly more than thermal displacements are far fewer in number and contribute a smaller force per atom to F_k . For example, with $v = 0.0005\sigma/t_{LJ}$ at $k_B T/\epsilon = 0$ only 0.3% of the monomers move by more than 0.12σ in $2t_{LJ}$. These monomers contribute less than 0.1% to the lateral force on the walls, and the percentage decreases as the velocity is lowered.

When the walls are commensurate, the distribution of metastable states depends on the relative positions of the walls. The number of atoms that pop between metastable states is a periodic function of the wall displacement. No pops occur when the walls are aligned directly above each other, and the total energy of the system is minimized in this configuration. The number of pops rises rapidly as the walls are moved out of alignment, and there are pronounced clusters of pops at unfavorable wall positions. The static friction is the maximum force exerted on the top wall at any position, while the kinetic friction represents an average over all wall positions. As a result, the two can be very different and the ratio depends on many factors including the length of the chains, number of chains, etc..

When the walls are incommensurate, the distribution of metastable states is independent of wall position. Thus the kinetic and static friction are correlated. The analogy to the Tomlinson model would suggest that the

kinetic and static friction should be equal in this limit. As illustrated above, this ratio depends on the velocity at which F_k is calculated and it may also depend on how F_s is calculated. Quoted results for F_s were obtained by determining the minimum force needed to produce a displacement of σ in a time $100t_{LJ}$. One might thus expect the results to correspond to an effective velocity of order $0.01\sigma/t_{LJ}$, and the static friction is indeed between the values of F_k for $v = 0.005$ and $0.05\sigma/t_{LJ}$. Rate-state models (Eqs. 3.1 and 3.2) also imply that the static friction depends on the time spent at zero velocity before a lateral force is applied. We are currently exploring the effect of waiting time on static friction and its relation to the velocity dependent kinetic friction.

4. Summary and Conclusions

We have examined the kinetic friction of surfaces separated by a layer of adsorbed molecules as a function of velocity, temperature, interaction potentials and surface alignment. The results are qualitatively consistent with many macroscopic measurements, and can be understood by analogy to simple model systems.

One of our main results is that the kinetic friction rises logarithmically with velocity. This dependence is commonly observed in experimental systems and is often associated with thermal activation [22,23,24]. Our analysis of the dynamics of individual monomers is consistent with this idea. We found that the kinetic friction was given by the force exerted by monomers that were trapped in metastable states. A simple argument shows that this force will decrease as v decreases.

The force from the top wall on a monomer in a given local potential well is zero at the bottom of the well. As it is displaced away from the minimum the force rises. When the force reaches its maximum value the monomer becomes unstable and pops to a new well. Since atoms that exert the largest force are closest to becoming unstable, they are the ones that are most likely to be thermally activated. When they hop to a new well, they contribute a smaller lateral force. As v decreases the time for thermal activation increases as σ/v . Thus more and more of the large contributions to F_k are lost due to thermal activation. As a result, F_k drops as v decreases.

Another important result is that adsorbed layers naturally lead to a kinetic friction that satisfies Eq. 1.1. He *et al.* had previously established this relation for the static friction [12]. Thus adsorbed layers provide a molecular basis for Bowden and Tabor's explanation of Amontons' laws in both contexts.

Changes in the kinetic friction with interaction potential and temperature closely parallel changes in the static friction. Both F_k and F_s are insensitive to parameters that are not controlled in typical experiments. Examples include wall orientation (θ), the num-

ber and precise size of adsorbed molecules, and even the strength of adsorption (ϵ_{wf}). This insensitivity is consistent with the fact that variations in the measured friction between nominally dry surfaces are relatively small ($\sim 25\%$). In contrast, simulations and analytic studies of bare surfaces show dramatic variations with surface orientation [4,5,6,7,8,9,10,11].

The linear relation between shear stress and pressure in Eq. 1.1 can be understood from a simple hard sphere picture (Fig. 4). The wall atoms create a surface of closest approach that adsorbed molecules must climb up in order to move laterally. The lateral force and normal force are related by the local slope of this surface, and α represents some average of the slope. Since ϵ_{wf} has little affect on the hard sphere diameter, changing it has little affect on α . In contrast, changing the ratio σ_{wf}/d_{mn} has a direct effect on both the slope and α (Figs. 3 and 4).

The simple hard sphere model also explains the insensitivity of α to the number of adsorbed molecules per unit surface area ρ [12,25]. Increasing the density of molecules spreads the normal pressure P and lateral stress τ over more molecules. However, the ratio between them, α , is still determined by the slope of the surface of closest approach. This surface is determined solely by the solids when the film is less than a monolayer thick. One only expects variations in α when the film becomes thicker than a monolayer and can shear internally. Preliminary studies of the thickness dependence do show such effects as the thickness increases to two or three layers.

The close connection between our results for kinetic and static friction is typical of experiments on nominally dry surfaces and surfaces that are purposely coated with thin hydrocarbon films [47]. We discussed how this connection can be understood from results for the simple Tomlinson model. Although the ratio $F_k(v)/F_s$ is relatively constant for a given velocity, there are noticeable changes with v due to the logarithmic variation in $F_k(v)$. We expect that the value of F_s will also vary logarithmically with the measurement time, and this remains an avenue for future research.

Another important focus of future research will be to improve the quantitative comparison between theory and experiment. The simulations described here use simple interaction potentials and surface geometries that capture qualitative features of the friction due to adsorbed layers. More detailed models of molecular structure and bonding, as well as surface roughness and elasticity will be needed to allow direct comparison to experiment.

Acknowledgements

The authors wish to thank Drs. M. H. Müser and P. M. McGuiggan for useful discussions. Support from

National Science Foundation Grant No. DMR-0083286 and from Intel Corporation through the donation of workstations is gratefully acknowledged.

References

- [1] G. A. Tomlinson, *Phil. Mag. Series 7* (1929) 905.
- [2] Y. I. Frenkel and T. Kontorova, *Zh. Eksp. Teor. Fiz.* 8 (1938) 1340.
- [3] G. M. McClelland, in *Adhesion and Friction*, edited by M. Grunze and H. J. Kreuzer (Springer Verlag, Berlin, 1989), Vol. 17, pp. 1–16.
- [4] M. Hirano and K. Shinjo, *Phys. Rev. B* 41 (1990) 11837.
- [5] M. R. Sørensen, K. W. Jacobsen, and P. Stoltze, *Phys. Rev. B* 53 (1996) 2101.
- [6] M. O. Robbins and E. D. Smith, *Langmuir* 12 (1996) 4543.
- [7] S. Aubry, in *Solitons and Condensed Matter Physics*, edited by A. R. Bishop and T. Schneider (Springer-Verlag, Berlin, 1979), pp. 264–290.
- [8] P. Bak, *Rep. Progr. Phys.* 45 (1982) 587.
- [9] M. Cieplak, E. D. Smith, and M. O. Robbins, *Science* 265 (1994) 1209.
- [10] M. O. Robbins and M. H. Müser, in *Handbook of Modern Tribology*, edited by B. Bhushan (CRC Press, Boca Raton, 2000 (cond-mat/0001056)).
- [11] M. O. Robbins, in *Jamming and Rheology: Constrained dynamics on microscopic and macroscopic scales*, edited by A. J. Liu and S. R. Nagel (Taylor and Francis, London, 2000 (cond-mat/9912337)).
- [12] G. He, M. H. Müser, and M. O. Robbins, *Science* 284 (1999) 1650.
- [13] M. H. Müser and M. O. Robbins, *Phys. Rev. B* 64 (2000) 2335.
- [14] M. H. Müser and M. O. Robbins, submitted to *Phys. Rev. Lett.* (cond-mat/0004494).
- [15] M. Godet, *Wear* 100 (1984) 437.
- [16] Y. Berthier, M. Brendle, and M. Godet, *STLE Tribology Trans.* 32 (1989) 490.
- [17] I. L. Singer, *Fundamentals of Friction: Macroscopic and Microscopic Processes* (Elsevier, Amsterdam, 1992), pp. 237–261.
- [18] F. P. Bowden and D. Tabor, *The Friction and Lubrication of Solids* (Clarendon Press, Oxford, 1986).
- [19] A. Volmer and T. Natterman, *Z. Phys. B* 104 (1997) 363.
- [20] J. A. Greenwood and J. B. P. Williamson, *Proc. Roy. Soc. A* 295 (1966) 300.
- [21] E. Rabinowicz, *Friction and Wear of Materials* (Wiley, New York, 1965).
- [22] J. H. Dieterich, *J. Geophys. Res.* 84 (1979) 2169.
- [23] A. Ruina, *J. Geophys. Res.* 88 (1983) 10359.
- [24] J. C. Gu, J. R. Rice, A. L. Ruina, and S. T. Tse, *J. Mech. Phys. Sol.* 32 (1984) 167.
- [25] G. He and M. O. Robbins, in preparation.
- [26] K. Kremer and G. S. Grest, *J. Chem. Phys.* 92 (1990) 5057.
- [27] W. Tschöp *et al.*, *Acta Polym.* 49 (1998) 61.
- [28] W. Tschöp *et al.*, *Acta Polym.* 49 (1998) 75.
- [29] M. P. Allen and D. J. Tildesley, *Computer Simulation of Liquids* (Clarendon Press, Oxford, 1987).
- [30] P. A. Thompson and M. O. Robbins, *Phys. Rev. A* 41 (1990) 6830.
- [31] M. J. Stevens and M. O. Robbins, *Phys. Rev. E* 48 (1993) 3778.
- [32] E. D. Smith, M. Cieplak, and M. O. Robbins, *Phys. Rev. B* 54 (1996) 8252.
- [33] E. Manias, G. Hadziioannou, and G. T. Brinke, *J. Chem. Phys.* 101 (1994) 1721.
- [34] R. Khare, J. J. de Pablo, and A. Yethiraj, *Macromolecules* 29 (1996) 7910.
- [35] G. S. Grest and K. Kremer, *Phys. Rev. A* 33 (1986) 3628.
- [36] J. H. Dieterich and B. D. Kilgore, *Tectonophysics* 256 (1996) 219.
- [37] Note that while increasing velocity always increases the friction at fixed Θ , the steady state kinetic friction may increase or decrease. From Eq. 3.2 the steady state of the system corresponds to $\Theta = D_c/v$, giving $\mu = \mu_0 + (A - B) \ln(v/v^0)$. This decreases with increasing velocity if $A < B$.
- [38] S. Granick, H. Hu, and G. A. Carson, *Langmuir* 10 (1994) 3867.
- [39] M. L. Gee, P. M. McGuiggan, J. N. Israelachvili, and A. M. Homola, *J. Chem. Phys.* 93 (1990) 1895.
- [40] I. Bitsanis, S. A. Somers, H. T. Davis, and M. Tirrell, *J. Chem. Phys.* 93 (1990) 3427.
- [41] P. A. Thompson, G. S. Grest, and M. O. Robbins, *Phys. Rev. Lett.* 68 (1992) 3448.
- [42] P. A. Thompson, M. O. Robbins, and G. S. Grest, *Israel J. of Chem.* 35 (1995) 93.
- [43] U. Landman, W. D. Luedtke, and J. Gao, *Langmuir* 12 (1996) 4514.
- [44] E. Manias, I. Bitsanis, G. Hadziioannou, and G. T. Brinke, *Europhys. Lett.* 33 (1996) 371.
- [45] M. O. Robbins and A. R. C. Baljon, in *Microstructure and Microtribology of Polymer Surfaces*, edited by V. V. Tsukruk and K. J. Wahl (American Chemical Society, Washington DC, 2000), pp. 91–117.
- [46] For submonolayer films the variation in α with θ is less than $\pm 15\%$.
- [47] B. N. J. Persson, *Sliding Friction: Physical Principles and Applications* (Springer, Berlin, 1998).